APPLIED MECHANICS MODELING OF GRANULATED CERAMIC POWDER COMPACTION

F. Michael Mahoney and Michael J. Readey
Glass and Electronic Ceramics Department
Sandia National Laboratories
Albuquerque, New Mexico 87185-0333

ABSTRACT

In ceramic manufacturing processes such as dry-pressing, correlations between applied compacting pressure and resultant powder compact density are essential for defining reliable process conditions for ceramic components. Pressure-density diagrams have been developed as a tool for both process control and for understanding the compaction behavior of different powders. These types of diagrams, however, pertain only to the average properties of a powder compact and do not address a significant issue in powder compaction processes: the formation of density gradients *within* the compact. Continuum-based mechanics models of varying complexity have addressed the influence of frictional forces acting at the powder-die wall interface which dissipate the applied pressure throughout the compact. Resulting pressure distribution models are then typically coupled with empirical functions relating pressure and density to obtain a green density distribution in the compact. All of these models predict similar trends; however, none predict the distribution with sufficient accuracy to be considered as a design tool for industrial applications.

KEY WORDS: Powder Compaction, Ceramic Materials, Modelling

1. INTRODUCTION

Most ceramic component manufacturing processes begin with a ceramic powder and a forming method to consolidate the powder into a desired shape. Shape-forming processes such as dry-pressing, slip-casting or injection-molding consolidate ceramic powders into porous compacts which are typically 60-70% dense. Complete densification of the porous compact occurs by subsequent sintering at high temperatures. Because of the large amount of porosity which must be eliminated, significant shrinkage accompanies densification. To achieve uniform shrinkage, homogeneous compaction of the ceramic powder is desirable. Variations in green body (consolidated) density will result in different amounts of shrinkage within the compact; lower density regions will either not densify completely or will shrink more than the surrounding regions, causing distortion or cracking during firing (1) .

The largest number of ceramic products are formed by pressing operations in which ceramic powder, placed in a die cavity, is compacted under an applied pressure acting in one direction (uniaxial pressing). Although high production rates can be achieved, it is well-known that dry-pressing of ceramic powders leads to density gradients in the pressed compact. Non-uniform

shrinkage during densification resulting from these density gradients necessitates diamond grinding to final dimensions which, in addition to being an extra processing step, increases the manufacturing cost of the product.

To develop methods to control and thus mitigate density variations in powder compacts, it has been the objective of researchers to better understand the mechanics of the compaction process and the underlying material and tooling effects on the formation of density gradients. This paper presents a review of a number of analyses and models existing in the literature related to the compaction behavior of ceramic powders under uniaxial pressing.

2. COMPACTION OF SPRAY-DRIED CERAMIC POWDERS

Starting ceramic powders used in manufacturing processes typically consist of submicron-sized, non-uniform-shaped particles. Such particles have low bulk densities and do not flow readily under compaction. To improve the flow behavior of the powder, submicron-sized particles are intentionally agglomerated into larger clusters by granulation (2).

Spray-drying is the most common technique for producing free-flowing granulated powder for pressing operations (2). A powder slurry containing a binder to provide green strength is sprayed into a chamber and falls through rising hot gases that evaporate the liquid (3). Liquid surface tension holds drops of the slurry in a spherical form. When dried, a distribution of ceramic powder granules are formed on the order of 100 μm in diameter, comparable to the size of powdered metals. However, unlike powdered metals which are dense, monolithic particles, each spray-dried ceramic granule is a porous composite consisting of original submicron-sized particles contained in a binder matrix. After spray-drying, the granulated ceramic powder is ready for consolidation.

Mechanical dry presses are often used for consolidation because of their high production rates and ease of automation. Figure 1 depicts the major steps used with this type of equipment. A predetermined amount of powder is introduced into the die cavity by a feed shoe [1]. The feed shoe retracts, smoothing the top surface of the die cavity [2] and the upper punch moves down to compact the powder [3]. After compaction, the upper punch retracts and the bottom punch ejects the compact from the die [4]. Depending on the size and complexity of the component, multiple punches can be set into motion and compaction can be carried out using both top and bottom punches (1).

3. PRESSURE-DENSITY DIAGRAMS

In dry-pressing operations, an applied compacting pressure yields a porous powder compact of a particular density which, in turn, determines the degree of shrinkage during densification. For process control, it is desirable to establish a quantitative relationship between the compacting pressure and the resultant compact density. For a given die dimension, the displacement of the upper punch (see Figure 1) can be used to calculate the change in volume of the powder compact as a function of applied pressure. For a constant mass of powder, the change in volume is directly related to the change in density (or porosity) of the compact. The general form of a pressure-density curve for granular material is shown in Figure 2. The ratio of changes in applied pressure to changes in density has been referred to as the compressibility factor of the powder (4).

The most complete approach to describing the compaction of ceramic powders would be to establish an analytical equation of state, relating pressure to volume in the powder compact. However, such an equation requires information such as the strength distribution of ceramic granules and particles, stress distributions between particle-particle and particle-binder interfaces and flow properties of granules under stress (3). Because of the difficulty in defining an accurate equation of state, empirical equations have been developed to fit pressure-density calibration curves as shown in Figure 2.

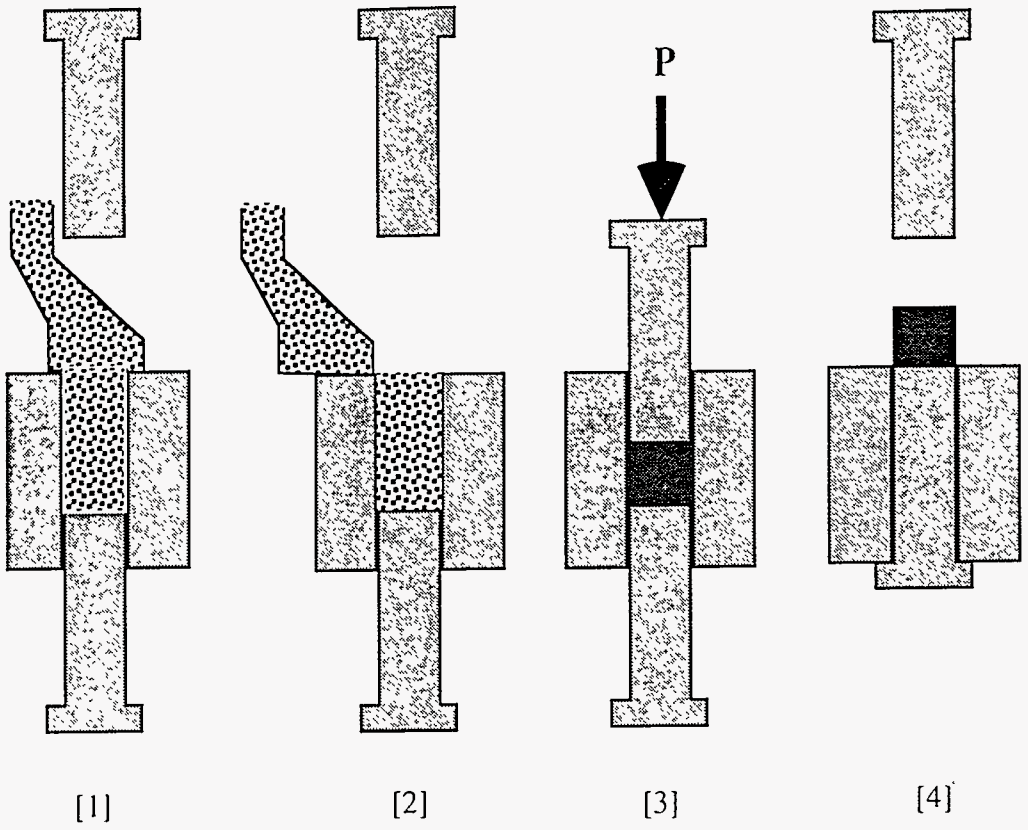

Figure 1. Stages of mechanical dry-press operation for powder consolidation: (1) die fill from feed shoe; (2) feed shoe retraction; (3) powder compaction; (4) die punch retraction and sample ejection. Adopted from Ref.[5].

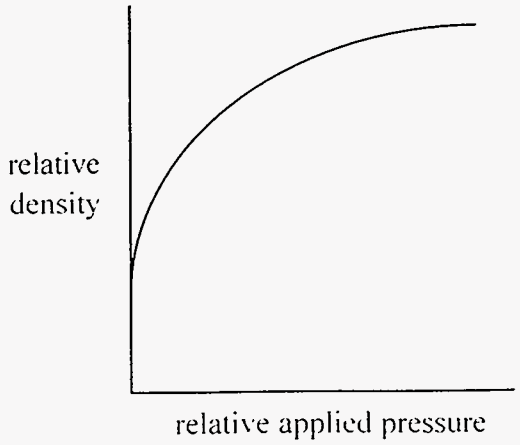

Figure 2. General form of applied pressure-density curve for granular material.

Several well-known empirical equations relate changes in density or porosity to exponential or power-law functions of the applied pressure(4,5):

$$\phi = \phi_o \exp\left[-\left(P_a/k_1\right)\right] \quad [1]$$

$$\rho_g = \rho_o + k_2 \cdot P_a^2 \quad [2]$$

$$\rho_g = \rho_o + k_3 \cdot P_a^{1/3} \quad [3]$$

where ϕ is porosity, ρ is density, P_a is applied pressure and the subscripts o and g refer to initial and green (consolidated) states, respectively. The constants k_1, k_2, and k_3 defined in the empirical equations reflect variations in material properties such as hardness and plasticity.

The pressure-density relationship has also been used to study the mechanisms of powder compaction. For example, Walker (6), Balshin (7) and Huffine and Bonilla (8) observed linear relationships between the logarithm of applied pressure and the volume of the powder compact for materials such as graphite, sodium carbonate and salts. Heckel (9) proposed an equation for the compaction of metals which Leiser and Whittemore (10) found to also fit the compaction behavior of pure fused magnesia, but not that of alumina, mullite or glass powders. Variations observed in compaction behavior suggest different mechanisms for different types of materials.

To more closely understand the compaction behavior of various powders, separate stages of compaction have been defined and specific mechanisms of compaction identified which act over particular stages. For granulated ceramic powders, the major stages of compaction are commonly defined as: [1] die-filling, in which powder flows into the die cavity and packs to fill density between 20-35%; [2] granule rearrangement under initial loading pressures where granules slide past one another and elastically deform; and [3] granule fracture in which fragmentation and plastic flow of granules occur. Although the various stages and mechanisms of compaction are easy to define, their distinction during the compaction process is difficult, since several mechanisms can act during any one stage and the different stages may overlap one another over a particular range of applied pressures.

In a study of several different ceramic powders*, Cooper and Eaton (11) divided the compaction response into two major stages: [1] the filling of large voids and [2] the filling of small voids which are depicted schematically in Figure 3. The filling of large voids corresponds to the mechanism of rearrangement where particles slide past each other to fill porosity on the order of the size of individual particles. The filling of small voids corresponds to the mechanisms of fragmentation and plastic flow in which individual particles fracture and deform to fill interstitial porosity much smaller than the sizes of individual particles.

These two stages of compaction are defined as independent, probabilistic processes. An equation to describe the compaction response for various materials was developed, in which the mechanisms acting over each of the two stages are defined as pressure-activated processes.

* the materials used in this study were bulk, non-agglomerated powders (not spray-dried granules) with a particle size distribution between 44-62 μm.

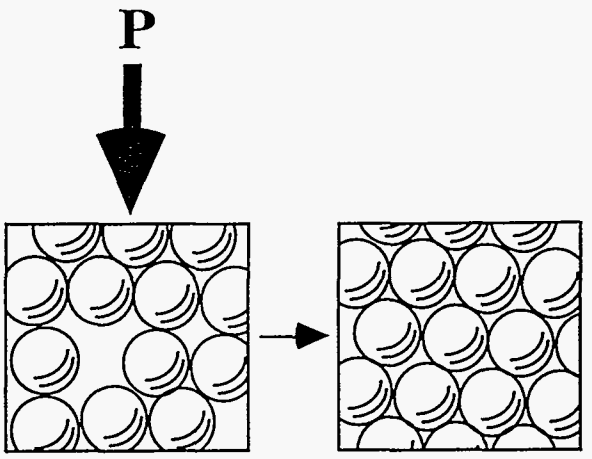

(a)

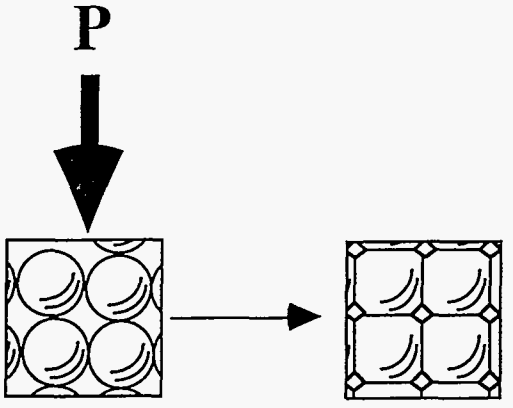

(b)

Figure 3. Major processes of powder compaction as defined by Cooper and Eaton (11): (a) the filling of large voids; (b) the filling of small voids

Decreases in the compact volume (increases in density) are equal to the sum of compaction achieved by each of the two stages identified:

$$V^* = a_1 \exp\left[-\left(k_4/P_a\right)\right] + a_2 \exp\left[-\left(k_5/P_a\right)\right] \qquad [4]$$

where

$$V^* = \frac{V_o - V}{V_o - V_\infty} = \%\ \text{total compaction}$$

$$a_1 \exp\left[-\left(k_4/P_a\right)\right] = \%\ \text{compaction associated with filling of large voids}$$

$$a_2 \exp\left[-\left(k_5/P_a\right)\right] = \%\ \text{compaction associated with filling of small voids}$$

The parameter V_o refers to the compact volume after die-filling, V_∞ is the compact volume at theoretical (highest) compaction and P_a is the applied pressure. The constants a_1 and a_2 represent the fraction of total compaction possible at infinite pressure by each particular void-

filling process; constants k_4 and k_5 are curve-fitting parameters based on pressures corresponding to the highest probabilities of filling each type of void. It should be noted that although the compaction behavior is separated into two different mechanisms, both act over the entire range of compacting pressures.

Another approach to describing the compaction response of ceramic powders was proposed by Lukasiewicz and Reed (12). Plotting the compaction diagram as %full density versus the logarithm of the applied pressure, the compaction behavior was separated into different stages by characteristic pressure levels as shown in Figure 4.

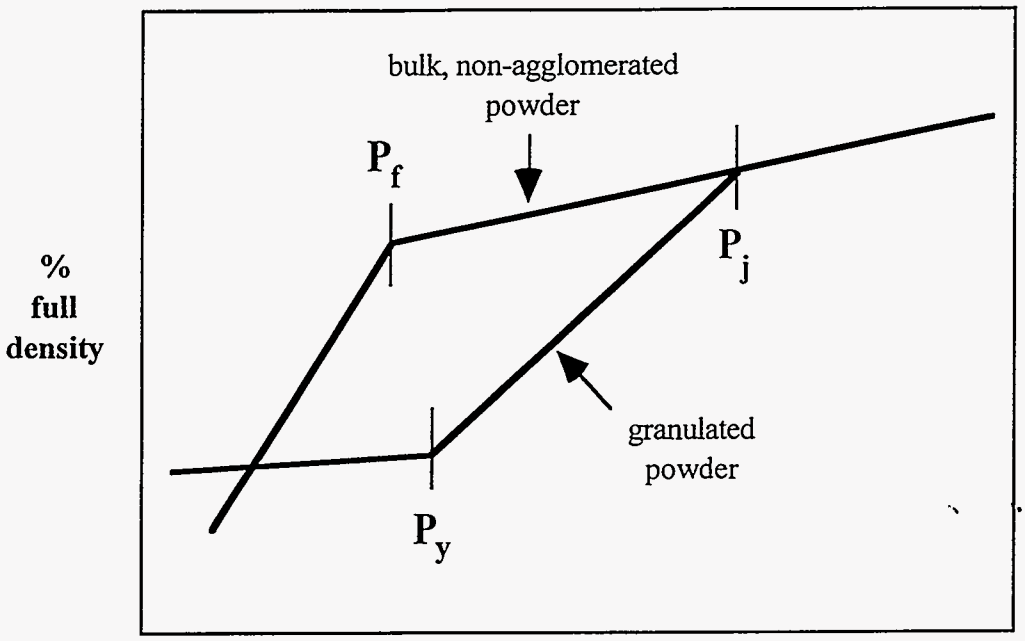

Figure 4. Logarithm pressure-relative density diagram used for identifying the compaction mechanisms of bulk and spray-dried ceramic powders. From Ref (12).

For bulk non-agglomerated powders, similar to those studied by Cooper and Eaton, two regions of compaction response are separated by the pressure required to fracture corners of particles in contact, P_f. This compaction behavior is similar to that defined by Cooper and Eaton in which the lower pressure region corresponds mainly to the filling of porosity on the order of individual particle sizes as particles rearrange by sliding past one another, but do not fracture. The higher pressure region above the particle fracture pressure corresponds to the filling of porosity much smaller than individual particle sizes as particles fragment or deform plastically. For spray-dried (granulated) ceramic powders, two different characteristic pressures were defined. The first is the apparent yield pressure of the spray-dried granules, P_y, below which only granule rearrangement and sliding occur. At this stage, the pore size distribution of the powder compact is bimodal, consisting of larger pores between granules (intergranular porosity) and smaller pores between individual particles *within* granules (intragranular porosity). Above the yield pressure, granules deform plastically to fill the intergranular porosity. As the compacting pressure increases, the intergranular porosity is continuously eliminated until the relative density of the granulated powder compact would be equal to the density of a bulk, non-agglomerated powder compact. At this "joining" pressure, P_j, the pore size distribution is unimodal; the intergranular and intragranular porosity distributions are similar. The compaction response above this pressure is the same for bulk as well as granulated powders. The characteristic compaction response shown in Figure 4 was observed for several different spray-dried (granulated) ceramic powders (12).

Many studies of compaction behavior based on pressure-density realtionships have been conducted and reviews of other powder compaction equations have been published (13,14). Although studies of pressure-density relationships are useful in elucidating the mechanisms by which compaction occurs, it is important to note that their results pertain only to the *average* properties of powder compacts. Moreover, the correlations established between applied pressure and density are largely empirical. More useful for modeling the compaction behavior is establishing a quantitative relationship between the applied pressure and the *density distribution* within a powder compact. To develop such a relationship, it is necessary first to establish a pressure distribution model for the compact as a function of applied pressure.

4. PRESSURE DISTRIBUTION IN POWDER COMPACTS

The geometry and compaction forces relevant to the uniaxial compaction of ceramic powders in a thick-walled cylindrical steel die is shown in Figure 5. For mechanics-based models, this geometry is easy to treat mathematically and generally consists of a compact of diameter D and height H.

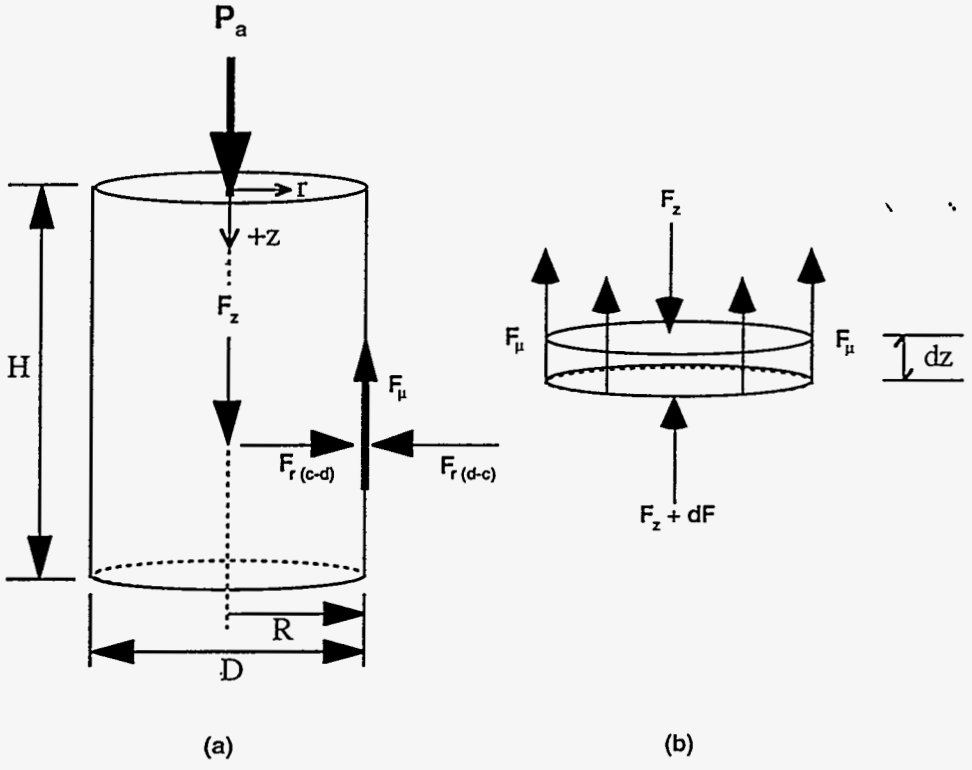

Figure 5. (a) Geometry and compaction forces related to cylindrical powder compact in pressing die.
(b) Forces acting on an axial slice of height *dz* at depth *z*

An applied pressure, P_a, acting over the top surface of the cylinder, will cause the powder to compact in the axial direction under the force, F_z. The applied pressure will also cause the compact to expand, but it is restricted by the die-walls, resulting in a radial force, F_r*. This radial force is commonly related directly to the axial force by a parameter α:

$$F_r = \alpha \cdot F_z \qquad [5]$$

* In Figure 5, the force $F_{r(c-d)}$ refers to the radial force of the powder compact on the die-wall; the force $F_{r(d-c)}$ refers to the reactive radial force of the die-wall on the powder compact.

For a solid material, the parameter α would be a function of the Poisson's ratio. For granular materials, α is an empirical factor representing bulk properties of the powder. The radial force against the die-wall subsequently generates a frictional force along the die-wall opposing the compacting pressure, P_a. This frictional force is related to the radial force by a powder/die-wall coefficient of friction, μ:

$$F_\mu = \mu \cdot \alpha \cdot F_z \qquad [6]$$

In this geometry, a cylindrical coordinate system is used with (positive) z in the (downward) axial direction and r in the radial direction.

4.1 Janssen Analysis of Pressure Distribution A related problem to the uniaxial compaction of powders was analyzed by H. A. Janssen who was concerned with pressure distributions within grain silos (15). Although his study was conducted 100 years ago, Janssen's work remains a classic analysis still used in many powder compaction studies today.

Janssen's analysis consisted of a force balance on an axial slice of a granular cylinder. The forces considered in this analysis, shown in Figure 5b, are the positive axial force, F_Z, resulting from the applied pressure, acting on the top surface of the axial slice; an opposing reactive force, F_Z+dF, acting on the bottom surface of the axial slice; and an opposing frictional force, F_μ, acting around the circumference of the axial slice:

$$F_z \downarrow - (F_z + dF) \uparrow - F_\mu \uparrow = 0 \qquad [7]$$

These forces are then set equal to pressures exerted over the area upon which they act:

$$\left(\pi D^2/4\right)(P_z) - \left(\pi D^2/4\right)(P_z + dP) - (\pi D \cdot dz)(P_\mu) = 0 \qquad [8]$$

From eq.[6], the die-wall frictional pressure can be related to the axial pressure,

$$P_\mu = \mu \cdot \alpha \cdot P_z \qquad [9]$$

Since all pressures are now related to the axial pressure, P_Z is simply set equal to P. Substituting eq.[9] into eq.[8] and rearranging yields,

$$\frac{dP}{P} = -\frac{4\mu\alpha}{D} dz \qquad [10]$$

Integrating this equation with respect to the axial direction from the top of the compact (z=0) yields,

$$\int_o^z \frac{dP}{P} = -\frac{4\mu\alpha}{D} \int_o^z dz \qquad [11]$$

$$\ln\left(\frac{P_z}{P_a}\right) = -\frac{4\mu\alpha}{D} z \qquad [12]$$

Equation [12] is then rearranged to yield Janssen's pressure distribution function,

$$P_z = P_a \exp\left(-\frac{4\mu\alpha}{D} z\right) \qquad [13]$$

which states that the axial pressure at any depth in the compact, P_Z, is equal to the applied compacting pressure, P_a, mutiplied by a term which decreases exponentially with depth into the compact.

The exponential term in eq.[13] includes both material and geometrical parameters. A closer examination of this relationship reveals two important trends. Firstly, if there is no friction at the die-wall ($\mu = 0$), the exponential term equals unity and the axial pressure is equal to the applied pressure throughout the compact. As the coefficient of friction increases, however, the axial pressure decreases exponentially with depth into the compact. It is important to note that this dissipation is entirely due to the opposing frictional force at the die-wall. Secondly, if the pressure decreases exponentially through the compact, then the aspect ratio of the compact must also have a significant influence. To show this effect, we can use eq.[13] to calculate the axial pressure at the bottom of a compact, P_H, for different aspect ratios (H/D, where z = H), assuming a constant die-wall coefficient of friction of 0.25 and an applied compaction pressure, P_a, of 68.9 MPa (10,000 psi). For example, a compact of aspect ratio 0.1 yields an axial pressure at the bottom of the compact of 65.6 MPa (9,510 psi). Thus, approximately 5% of the applied compacting pressure is dissipated from the top of the compact to the bottom. For an aspect ratio of 1, P_H = 41.8 MPa (6,065 psi); approximately 40% of the applied pressure is dissipated at the bottom of the compact. Increasing the aspect ratio to 4, almost 87% of the axial pressure acting on the top surface will be dissipated within the powder compact (P_H = 9.3 MPa (1,350 psi))!

Explicit in Janssen's analysis is the fact that the axial pressure at any depth into the compact is constant along that plane. That is, no variations in pressure occur with respect to radius from the center of the plane out to the die-wall because variation of F_r with respect to radial position is ignored. According to this pressure distribution model, differences in green body density should only be evident with respect to axial position in a compact.

4.2 Thompson Analysis of Pressure Distribution A mathematical model to account for pressure variations with respect to *radial* position was developed by Thompson (16) beginning with the equilibrium equation for stresses acting on a cylindrical compact in the axial direction,

$$\frac{\partial \tau}{\partial r} + \frac{\partial \sigma_z}{\partial z} + \frac{1}{r}\tau = 0 \qquad [14]$$

This equation includes an axial stress term (σ_z) and a shear stress term (τ); no variation in the θ direction is observed due to radial symmetry. Rearranging this equation, Thompson defined a relationship for the axial stress with respect to the axial direction:

$$\frac{\partial \sigma_z}{\partial z} = \frac{1}{r}\frac{\partial}{\partial r}(r\tau) \qquad [15]$$

Next, variation of this axial stress with respect to the radial direction is taken into account. Evidence for such a radial dependence came from experimental data generated by Unckel (17) who measured density as a function of position in metal powder compacts and postulated that the radial pressure distribution necessary to account for these variations was parabolic about the central axis at any depth in the compact. Using Unckel's experimental results, Thompson empirically fit a parabolic radial dependence to the axial stress,

$$\sigma_z(r,z) = r^2 f(z) + C(z) \qquad [16]$$

where C(z) represents the stress along the central axis (at $r = 0$). Assuming that the shear stress is also some function of both r and z, Thompson solved for eq.[15] by setting boundary conditions for the shear stress: at the die-wall ($r = R$), the shear stress is equal to the familiar relationship of the radial force times the coefficient of friction (from eq.[6]). Because of radial symmetry, Thompson states that the shear stress is zero along the central axis. He then

concludes by inspection of eq.[15] that the axial stress along the central axis must be constant, independent of z*. Thus, $C(z)$ is equal to C. The resulting equation,

$$\sigma_z(r,z) = B\left(\frac{r^2}{R^2}\right)\exp\left(-\frac{4\mu\alpha}{R}z\right) + C\left(1-\frac{r^2}{R^2}\right) \qquad [17]$$

contains two terms. The first term includes the same exponential term found in Janssen's analysis (eq.[13]). Additionally, there is a radial term which includes the radial distance from the central axis, r, and the radius of the compact, R. This term also influences the exponential term.

Based on the analyses of Janssen and Thompson, it is evident that a pressure applied to the top of a powder compact generates a pressure distribution within the compact which varies in both the axial and radial directions.

An important consequence of this pressure distribution is evident from inspection of the pressure-density diagram in Figure 4. Differences in pressure will obviously result in differences in green body density within the compact. Furthermore, the pressure distribution will result in different mechanisms controlling the consolidation of the powder in different regions within the compact.

5. DENSITY DISTRIBUTION IN POWDER COMPACTS

Mechanics-based analyses have been used to determine pressure distributions in a powder compact as shown by Janssen and Thompson. To predict density distributions in a powder compact under an applied pressure, pressure distribution functions must be coupled with some form of a pressure-density relationship such as described in Section 3. Thompson established a density distribution model by substituting his stress (pressure) distribution function (eq.[17]) into a general empirical stress(pressure)-density relationship (eq.[3]). The result is shown in Figure 6 with lines of constant density for a powder compact of aspect ratio 1.

Several notable trends can be observed in the density distribution predicted by Thompson's model. First, in the near die-wall region ($r \approx R$), the density decreases in the axial direction from the top to the bottom of the compact. The highest density is found at the top of the compact at the die-wall; the lowest density is at the bottom of the compact at the die-wall. This trend is qualitatively similar to the trend of decreasing pressure in the axial direction predicted by Janssen's analysis. Secondly, in the radial direction, Thompson's model predicts increasing density from the central axis to the edge of the compact in the top region of the sample. This radial dependence in density continues with distance from the top surface down into the compact until a plane of constant density is reached near the middle of the sample. Below the plane of constant density, the radial dependence reverses and density *decreases* from the central axis to the edge of the sample. Finally, the density distribution model predicts a constant density along the central axis of compact in the axial direction.

Validation of the density distribution model can be made by comparison with the limited experimental results available. Density distribution maps similar to Figure 6 have been generated experimentally for powder compacts of comparable aspect ratio. Kuczynski and Zaplatynskyj (18) conducted compaction tests on nickel powder and measured the hardness as a function of position on an axial slice of the compact. After establishing a hardness-density calibration curve for nickel, the density distribution as a function of position was plotted. Train (19) used powder displacement and direct weight/volume measurements to determine the

---

* While it is true that the shear stress is zero at r=0, it does not follow that the derivative of σ_z with respect to z must also be zero along the central axis. Thompson's approach is valid only for a limited case; a more general mechanics analysis reveals a non-zero derivative of σ_z at r=0, indicating that C(z) is indeed a function of z and not constant.

density distribution within magnesium carbonate powder compacts. The results of these two studies are shown in Figure 7.

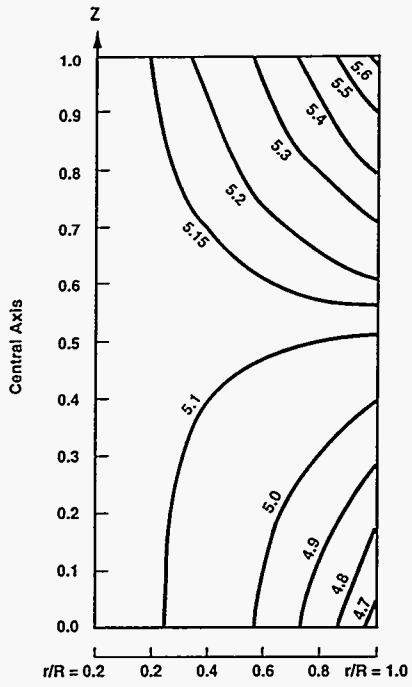

Figure 6. Lines of constant density for a powder compact with $\alpha = 0.5$, $\mu = 0.3$, and H/D = 1 [from Ref. (16)]

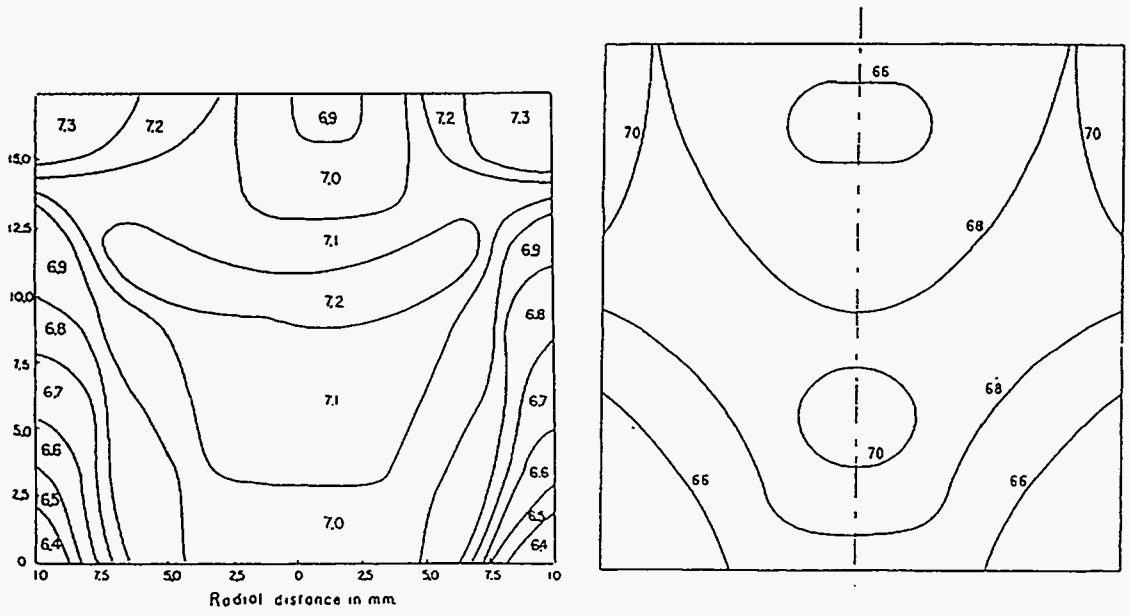

(a) (b)

Figure 7. Density distribution maps determined from experimental measurements
(a) Nickel powder compacted under 0.32 MPa (46 psi) pressure
(b) Magnesium carbonate powder compacted under 2040 kg/cm^2 pressure

Compared with the experimental results, the density distribution predicted by Thompson's model agrees well in several areas. In the near die-wall region, decreasing density in the axial direction is predicted by the model and found experimentally. Also, the predicted increase in density with radial position from the central axis to the edge of the compact at the *top* of the compact, and the decrease in density with radial position at the *bottom* of the compact are also qualitatively similar to trends observed experimentally. However, the model predicts a constant density along the central axis which does not match results found experimentally. In both density maps shown in Figure 7 and in measurements made by Unckel (17), regions of density maxima were observed in the bulk of powder compacts.

Another model for predicting density distributions in pressed powder compacts was developed by Schwartz and Weinstein (20) who proposed the application of a Coulomb yield criterion to describe the compacton of granular material. Although their analytical approach differed from that of Thompson, a qualitatively similar stress distribution resulted with a constant stress predicted along the central axis. Thus, comparison of model predictions with experimental results indicates that existing compaction models are capable of predicting accurate trends in the near-surface region of pressed powder compacts, but fail to capture the complexities of density variations in the bulk of the compact. It should also be noted that the two models described above are limited to cylindrical geometries.

Simulation of compaction using other finite element methods with associated constitutive laws for material behavior (i.e., elastic, plastic, viscoelastic, etc.) are also emerging (21-23). These approaches allow examination of more complex geometries, but still only provide insight into trends, mainly because all the models still consider die-wall frictional forces as the only source of pressure dissipation during the compaction process. Sufficient evidence now exists that *interparticle* friction is also important in the development of density gradients (24,25). Thus, it appears that additional interparticle mechanisms or dissipative forces to the die-wall frictional force must be taken into account in any model which aims to accurately predict density gradients in ceramic powder compacts.

6. SUMMARY

Numerous analyses and models exist in the literature for investigating and predicting the compaction behavior of ceramic powders. Pressure-density diagrams have been developed as a tool for both process control and for elucidating compaction mechanisms which act under different ranges of applied pressure. It is important to note, however, that such diagrams pertain only to the average properties of powder compacts. To better understand the significant issue of density variations within pressed powder compacts, models of pressure distribution resulting from an applied compacting pressure have been developed. Coupling pressure distribution functions with pressure-density relationships allows the development of models to predict density distributions. Comparison of model predictions with experimental results, however, points to the need for a more thorough understanding of the underlying mechanics describing compaction to develop models with more accurate predictive capability.

Acknowledgements

This work was performed at Sandia National Laboratories, and was supported by the U.S. Department of Energy under Contract Number DE-AC04-94AL85000.

1. D. W. Richerson, Modern Ceramic Engineering: Properties, Processing and Use in Design; 2nd ed.; Marcel Dekker, Inc.: New York, 1992, pp 435, 437.

2. S. J. Lukasiewicz in Engineered Materials Handbook: Volume 4, Ceramics and Glasses, ASM International, 1991, pp. 100-107.

3. O. J. Whittemore Jr. in G. O. Onoda Jr. and L. L. Hench, eds., Ceramic Processing Before Firing, John Wiley & Sons, Inc., New York, 1978, pp. 343-355.

4. G. B. Smith, Met. Ind., 72, 427 (1948).

5. R. P. Seelig, Trans. Inst. Min. Metall., 171, 506-517 (1947).

6. E. E. Walker, Trans. Faraday Soc., 19, 73 (1923).

7. M. Y. Balshin, Vestnik Metalloprom, 18, 124-37 (1938).

8. C. L. Huffine and C. F. Bonilla, Amer. Inst. Chem. Eng. J., 8, 490-93 (1962).

9. R. W. Heckel, AIME Trans., 221, 1001-1008 (1961).

10. D. B. Leiser and O. J. Whittemore Jr., Am. Ceram. Soc. Bull., 49, 714-17 (1970).

11. A. R. Cooper and L. E. Eaton, J. Am. Ceram. Soc., 45, 97-101 (1962).

12. S. J. Lukasiewicz and J. S. Reed, Am. Ceram. Soc. Bull., 57, 798-801 (1978).

13. K. Kawakita and K.-H. Lüdde, Powder Technology, 4, 61-68 (1970/71).

14. W. Chen and S. G. Malghan, Powder Technology, 81, 75-81 (1994).

15. H. A. Janssen, Zeit. d. Vereins Deutsch. Ing., 39, 1045-49 (1895).

16. R. A. Thompson, Am. Ceram. Soc. Bull., 60, 237-243 (1981).

17. H. Unckel, Archiv für das Eisenhüttenwesen, 18, 161-67 (1945).

18. G. C. Kuczynski and I. Zaplatynskyj, Journal of Metals, February, 215 (1956).

19. M. C. Train, Trans. Instn. Chem. Engrs., 35, 258-66 (1957).

20. E. G. Schwartz and A. S. Weinstein, J. Am. Ceram. Soc., 48, 346-50 (1965).

21. S. Shima and K. Mimura, Int. J. Mech. Sci., 28, 53-59 (1986).

22. G. G. Weber and S. B. Brown in Advances in Powder Metallurgy, Metal Powder Industries Federation, Princeton, N. J., 1989; Vol. 105-118.

23. R. W. Lewis and A. G. K. Jinka and D. T. Gethin, Powder Metallurgy Industry, 25, 287-293 (1993).

24. G. G. W. Mustoe and G. L. DePoorter and D. R. Greening, International Conference on Advanced Synthesis of Engineered Structural Materials, San Francisco, CA, ASM International, 1992, pp. 73-79.

25. F. M. Mahoney and M. J. Readey in J. J. Kingsley, ed., Symposium on Science, Technology and Commercialization of Powder Synthesis and Shape Forming Processes, Cincinnati, OH, American Ceramic Society, 1995.

DISCLAIMER